agriculture

MDPI

Article

Simulation Analysis and Parameter Optimization of Seed–Flesh Separation Process of Seed Melon Crushing and Seed Extraction Separator Based on DEM

Qi Luo [1], Xiaopeng Huang [1], Jinfeng Wu [1], Xiaobin Mou [1], Yanrui Xu [1], Shengyuan Li [1], Guojun Ma [1], Fangxin Wan [1,*] and Lizeng Peng [2,*]

[1] College of Mechanical and Electrical Engineering, Gansu Agricultural University, Lanzhou 730070, China; luoqi@gsau.edu.cn (Q.L.); huangxp@gsau.edu.cn (X.H.); wujf@gsau.edu.cn (J.W.); mouxb@gsau.edu.cn (X.M.); xuyr@st.gsau.edu.cn (Y.X.); hecunc@st.gsau.edu.cn (S.L.); magj@gsau.edu.cn (G.M.)

[2] Key Laboratory of Agro-Products Processing Technology of Shandong Province, Key Laboratory of Novel Food Resources Processing Ministry of Agriculture, Institute of Food and Nutrition Science and Technology, Shandong Academy of Agricultural Sciences, 23788, Gongye NRd, Licheng District, Jinan 250100, China

* Correspondence: wanfx@gsau.edu.cn (F.W.); penglizeng@sdnu.edu.cn (L.P.); Tel.: +86-138-9316-3871 (F.W.); +86-159-5412-8918 (L.P.)

Abstract: In order to enhance the comprehensive processing quality and production efficiency of seed melons, a seed melon crushing and seed-extraction separator has been developed and designed. Aiming at the issues of high impurity rate and scratch rate of melon seeds in the process of seed–flesh separation, the structure and parameters of the seed–flesh separation device were optimized in this study by simulation analysis and field testing. The simulation model of melon seed, melon flesh, and the seed–flesh separation device based on the discrete element method (DEM) was established, and the simulation parameters were calibrated. Subsequently, the melon seed impurity rate (G_1) and the melon seed scratch rate (G_2) were used as the evaluation indexes. The single-factor simulation test was carried out on the separation roller speed (A). The spacing between the scraper and the screen (B), the separation roller scraper inclination angle (C), and the influence rules of each factor on the separation effect of the seed–flesh were obtained. Finally, the three-factor and three-level orthogonal test was carried out. Using the method of ANOVA and multi-objective optimization, the optimal working parameters of the device were obtained as A-117.53 r/min, B-5 mm, and C-10°, at which time the optimal evaluation indexes were G_1-5.59% and G_2-2.85%. The prototype test was carried out with the optimization results. The values of G_1 and G_2 were measured at 5.71% and 2.91%, respectively, and the relative errors with the simulation values were 2.15% and 2.11%, respectively, which were basically the same between the simulation model and the prototype test. The results indicate that the designed separation roller speed, spacing between the scraper and screen, and separation roller scraper inclination angle can meet the requirements of seed–flesh separation in the seed melon crushing and seed-extraction separator. The results of the DEM study can provide a reference for the optimal design of the seed–flesh separation device.

Keywords: seed melon; seed–flesh separation device; discrete element method (DEM); multi-objective optimization; prototype test

Citation: Luo, Q.; Huang, X.; Wu, J.; Mou, X.; Xu, Y.; Li, S.; Ma, G.; Wan, F.; Peng, L. Simulation Analysis and Parameter Optimization of Seed–Flesh Separation Process of Seed Melon Crushing and Seed Extraction Separator Based on DEM. *Agriculture* **2024**, *14*, 1008. https://doi.org/10.3390/agriculture14071008

Academic Editor: Mustafa Ucgul

Received: 26 May 2024
Revised: 22 June 2024
Accepted: 23 June 2024
Published: 26 June 2024

1. Introduction

Seed melon is a variety of low-sugar melon, a type of watermelon. Originally native to the Kalahari Desert in Africa, it was subsequently introduced to China. Currently, seed melon is among the melon crops extensively cultivated in the northwest region of China [1]. A seed melon consists of three parts: the melon peel, melon flesh, and melon seeds. The melon flesh can be utilized in the production of seed melon water, juice, and various other products. The melon seeds are processed into a popular snack. Despite this,

the benefits of seed melon have long been underestimated. The traditional utilization of seed melon is manually extracting the melon seeds, which account for only 3% to 5% of the fresh melon's weight from the melon flesh, while over 95% of the melon flesh and melon peel are casually discarded in fields and ditches. This not only results in resource wastage but also environmental pollution [2–4]. The comprehensive utilization technology of seed melons enables the crushing, separation, and deep processing of the peel, flesh, and seeds of the seed melon, thereby fully utilizing its components. However, existing equipment in the seed–flesh separation process for melon seeds is currently causing a high rate of impurity and significant damage to the seeds, which in turn severely hinders the development of the industry. Consequently, there is a pressing need to optimize the operational parameters of the seed–flesh separation device within the seed melon crushing and seed-extraction separator.

Currently, the academic literature concerning the crushing and separation devices for agricultural materials has made notable advancements. However, the majority of research in this field is centered on major crops like fruits, vegetables, and grains. Regrettably, there is a lack of literature exploring the separation of seed and flesh in seed melon. For example, Wu et al. [5] conducted an experiment to optimize the oilseed rape threshing and separating device based on the discrete element method (DEM). The results indicated that the threshing cylinder speed, concave plate speed, and guide plate angle were influencing factors. Zhang et al. [6] aimed at the problems of a low threshing rate and a high loss rate in the threshing and separating device of a millet combine harvester; they designed an axial-flow threshing and separating device with a front-end rasp bar and rear-end nail tooth structure. The DEM simulation was carried out to assess the influence of rotary roller speed, threshing clearance, and concave grid spacing on the operation performance. Wang et al. [7] developed a modeling and simulation method for the threshing process of rice plants based on the DEM. The simulation could predict the effects of the feed rate, cylinder speed, threshing gap, and rolling friction on the threshing performance. Coetzee et al. [8] developed a model of a bunch of grapes and a model of a commercial destemmer based on the DEM, which could accurately predict the amount of berries removed from the bunches, the spatial distribution of berries, and the impurity rate within the berries at the discharge. Li et al. [9] developed a longitudinal axial flow staggered flexible threshing device for millet. Through DEM simulation, the results showed that with the feed volume was 1.3 kg/s, the drum speed was 762 r/min^{-1}, the threshing clearance was 15 mm, the agglomeration rate was 2.92%, the loss rate was 1.58%, and the damage rate was 0.37%. Ma et al. [10] simulated the motion and separation process of grain and straw mixtures in a variable-amplitude sieve box with three degrees of freedom (two translational and one rotational) using the discrete element method. The results showed that the mixtures in the front section of the sieve screen were quickly thrown up and moved back. The separation process primarily occurred in the middle and rear sections of the sieve screen but could not favor their segregation and separation at the front section of the sieve screen. The research on the performance of seed–flesh separation may refer to the research conducted on particle separation performance by relevant scholars. For example, Yu et al. [11] used the discrete element method (DEM) to analyze the screening process in the vibrating flip–flow screens (VFFS). Through simulation, the flow and separation behaviors of particles of varying sizes in the VFFS were identified, and the validity of the simulation was confirmed with pilot-scale screening tests. You et al. [12] used the discrete element method (DEM) to simulate the motion behavior of spherical and non-spherical particles on an inclined vibrating plate and investigated how different operating parameters affected the separation efficiency of mixed particles.

Constructing discrete elemental models of melon seeds and melon flesh that closely represent the actual situation can enhance the accuracy of simulation results. At the same time, this approach also results in a considerable increase in simulation workload. Therefore, it is essential to solve this problem by simplifying the model. Ghodki et al. [13] used the DEM to establish the model of black pepper seed by many spherical particles through

Hertz–Mindlin with bonding and omitted the structure of the seed coat and endosperm. Wang et al. [14] simplified the straw of citrus fruits into a cylindrical model, and a discrete element model for citrus fruit stalk with a 3 mm diameter was established using the DEM. Su et al. [15] proposed a simplified method to build a discrete elemental model of flexible rice straw and arranged several soft particles in a radial cycle along the straw and in order along the straw axis using the DEM particle factory. The macroscopic kinematic behavior observed in particulate matter is the result of the physical properties of the particles and the interactions between the particles and the surrounding environment. These interactions include the intrinsic characteristics of the particles and the contact parameters between the particles and the external surroundings. For example, Horabik and Molenda [16] discussed the advancements in research concerning the discrete elemental models and contact parameters for agricultural particulate materials. The development of a precise model and the utilization of accurate contact parameters significantly impact simulation outcomes, and certain physical characteristics of particles can be determined through direct measurements. Liu et al. [17] established the flexible discrete element model of wheat hollow short straws based on the DEM, employed the Hertz–Mindlin with a bonding contact model, and conducted the calibration of various parameters. Song et al. [18] selected the angle of repose (AoR) and the bulk height as macroscopic response indicators based on particle stacking tests and numerical simulations, and they calibrated six contact parameters frequently applied in DEM simulations of fertilizer particles using the designing of experiments (DoE) method.

In summary, several studies have explored the application of the discrete element method (DEM) in the mechanical separation of cereals, rice, corn, grapes, and other crops. This paper, based on the discrete element simulation research method of mechanical separation of these crops, takes the self-developed seed melon crushing and seed-extraction separator as a prototype and takes the seed–flesh separation device as a research object to simulate and optimize the seed–flesh separating process and carry out experimental research. The DEM model is established for melon seeds, melon flesh, and the seed–flesh separation device. Key parameters, such as the separation roller speed, spacing between scraper and screen, and the separation roller scraper inclination angle, are analyzed using single-factor and three-factor three-level orthogonal tests to assess their impact on seed–flesh separation effectiveness. A multi-objective optimization approach is employed to develop a regression model correlating evaluation indexes with influencing factors, thereby determining the optimal working parameter combination for the seed–flesh separation device. This research outcome will provide valuable insights for future design considerations regarding the operational parameters and structural configurations of the seed–flesh separation device of seed melon crushing and seed-extraction separator.

2. Materials and Methods

In this study, the "Jingyuan No. 1" variety of seed melon planted in a dry sand field in Gaowan Town, Jingyuan County, Baiyin City, Gansu Province, was chosen as the focal point. Both its melon seeds and flesh were the main object of the study, as shown in Figure 1. The QW-QZ-2 seed melon crushing and seed-extraction separator, which was independently researched, developed, and designed by the study group, was used as a prototype. This prototype can realize the crushing of seed melons and the separation operation of the components of the skin, flesh, and seeds, as shown in Figure 2. The structure and parameters of the seed–flesh separation device with the seed melon crushing and seed-extraction separator were optimized, as shown in Figure 3.

Figure 1. Seed melon and cross-section. (1) Melon seed; and (2) melon flesh.

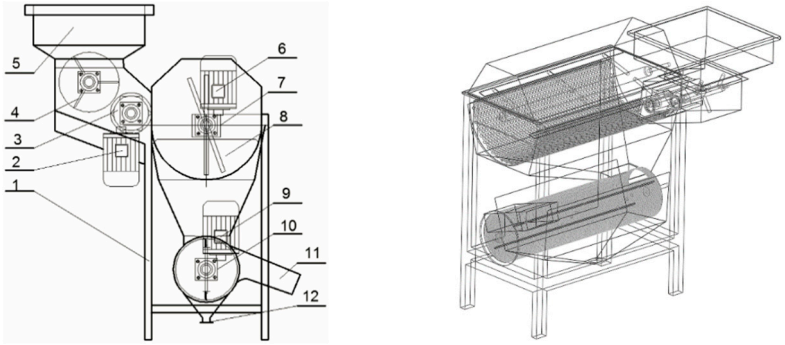

Figure 2. The whole machine structure and three-dimensional model of seed melon crushing and seed-extraction separator. (1) Frame; (2) motor I; (3) extrusion roller; (4) seed melon crushing toothed roller; (5) feeding hopper; (6) motor II; (7) melon skin–flesh separation device; (8) melon skin outlet; (9) motor III; (10) seed–flesh separation device; (11) melon seed outlet; and (12) melon juice outlet.

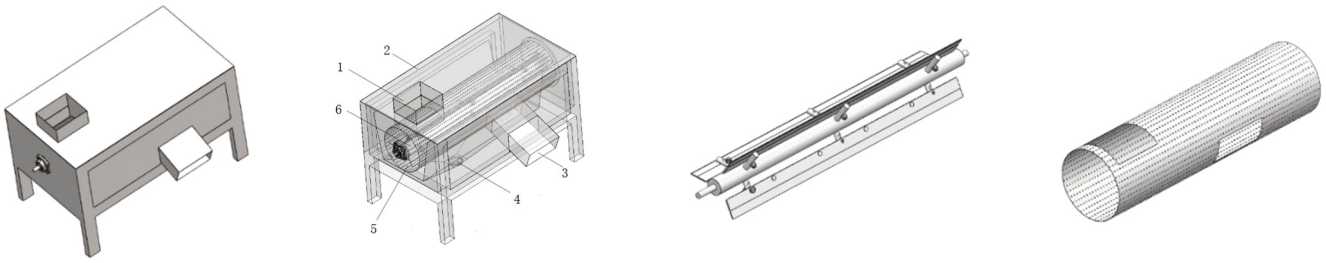

(**a**) (**b**) (**c**)

Figure 3. The seed–flesh separation device. (**a**) (1) Inlet; (2) frame; (3) melon seed outlet; (4) melon juice outlet; (5) separation screen; and (6) separation roller. (**b**) Separation roller. (**c**) Separation screen.

2.1. Structure of the Seed–Flesh Separation Device and Its Arrangement in the Whole Machine

2.1.1. The Whole Machine Structure of Seed Melon Crushing and Seed-Extraction Separator

Seed melon crushing and seed-extraction separator consist of a feeding inlet, crushing and extruding device, skin–flesh separating device, seed–flesh separating device, transmission device, motor, and frame. The structure of the whole machine is shown in Figure 2.

When the machine is working, a seed melon is put into the feeding hopper of the machine. The seed melon crushing toothed roller and the pressure roller rotate at specific speeds relative to each other so that the seed melon can be extruded and transported in time after the whole melon is crushed. After the above action, the seed melon has initially realized the separation of melon skin, seeds, and flesh, forming an uneven medium mixture. Under the action of the melon skin–flesh separating roller in the melon skin–flesh separating device, the melon skin in the seed mixture is further broken, dividing the mixture into two components: the crushed skin is ejected from the apparatus through the melon peel outlet, while the seed–flesh mixture descends into the seed–flesh separation device with the aid of

the separating roller's compression and mechanical agitation through peel–flesh separation device. Subsequently, under the assistance of the seed–flesh separating roller, the melon flesh is further broken, passes through the seed–flesh separating screen, and comes out from the melon juice outlet. The melon seeds, which are larger in size, do not pass through the screen and instead exit through the melon seed outlet due to axial force. Through the above process, the separation of the skin, flesh, and seeds of the seed melon is realized, which can provide different components of raw materials for subsequent processing.

Considering the present state of the seed melon crushing and seed-extraction separator, the primary technical parameters of the machine are outlined in Table 1 to maintain machine quality and operational safety.

Table 1. Main technical parameters of the whole machine.

Technical Parameters	Value
Weight of the whole machine (kg)	500
Matching power (KW)	4.5
Production capacity ($t \cdot h^{-1}$)	1.5–2
Appearance size (length·width·height) (mm)	1460 × 1350 × 1735
Material	SUS304

2.1.2. Structure of the Seed–Flesh Separation Device

The melon seed–flesh separation device constitutes the lower segment of the seed melon crushing and seed-extraction separator. It is designed in the structure of an axial-flow roller type, which includes components such as the inlet, separation rollers, separation screen, and a melon seed and flesh discharge outlet. The independent structural layout of this device is shown in Figure 3a. In the working process, the mixture of seeds and flesh is introduced into the seed–flesh separation device from the skin–flesh separator, entering through the feeding port 1. The separating roller rotates at a certain rotational speed and, under the axial and tangential forces exerted by the scraper, compresses the seed–flesh mixture, leading to further crushing and finely dividing of the melon pulp. Subsequently, the fragmented melon flesh passes through the mesh apertures of the separating screen, exiting through the melon juice outlet, while the melon seeds are directed toward the melon seed outlet, thereby achieving the final separation of the melon seeds and flesh.

The key components of the seed–flesh separating device comprise a seed–flesh separation roller and a seed–flesh separation screen. The separation roller was comprised of the roller shaft, the support bar, and three scrapers, as shown in Figure 3b. The three scrapers are evenly distributed along the circumference of the roller shaft, with a pinch angle of 120° and a length of 1150 mm, and a 10 mm thick food-grade soft silicone pad is affixed in the center of the scrapers to reduce the likelihood of melon seed damage. The seed–flesh separation screen, designed cylindrically as shown in Figure 3c, features a screen diameter of 300 mm and an aperture diameter of 6 mm.

2.2. Simulation Modeling Based on DEM

2.2.1. Simulation Model of Seed Melon Components

Cundall and Strack (1979) introduced the discrete element method (DEM) as a numerical simulation approach to analyze the mechanical characteristics of granular materials. This method, grounded in Newton's second law and Euler's equations, has proven to be an effective tool for predicting the kinematic behavior of granular materials with precision [19]. Due to its accuracy and efficiency, DEM has found extensive applications in research related to agricultural machinery [20–24].

A discrete element model of the seed melon components was developed in DEM 2022. Assuming that melon seeds and melon flesh are influenced by interparticle bonding forces, their shape, and size adhere to sample statistics. They are filled with spherical particles, each with a radius of 2 mm and a radius multiplier ranging from 0.8 to 1.2. The discrete elemental model of melon seeds and flesh is depicted in Figure 4.

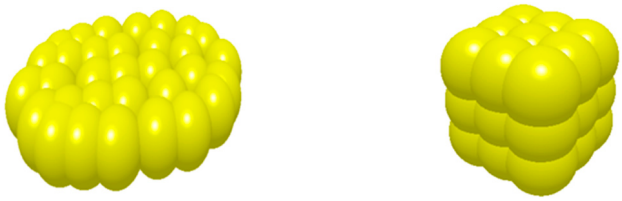

(**a**) (**b**)

Figure 4. Discrete element model of seed melon components. (**a**) Discrete elemental model of melon seed. (**b**) Discrete elemental model of melon flesh.

2.2.2. Simulation Model of the Seed–Flesh Separation Device

A discrete element model of the seed–flesh separation device was developed in DEM 2022, illustrated in Figure 5. The model includes essential components such as the separation rollers, screen, casing, inlet, and outlet, all fabricated from 304 stainless steel.

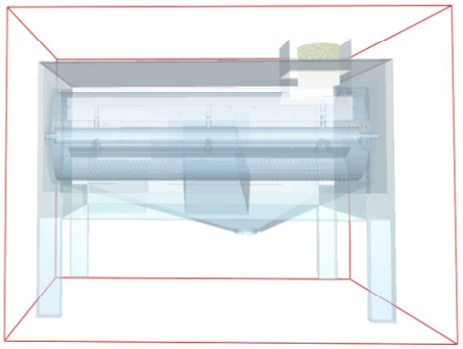

Figure 5. Discrete element model of the seed–flesh separation device.

2.3. Calibration of Simulation Parameters

2.3.1. Calibration of Intrinsic Parameters

Intrinsic parameters are an essential property of a material and generally do not change with particle volume and shape. The intrinsic parameters to be examined in this study encompass the size, density, Poisson's ratio, and shear modulus of both melon seeds and melon flesh [18].

To establish an accurate discrete element model of melon seeds and flesh, test samples comprising melon seeds (200 pieces) and corresponding flesh were selected based on previous research by the group [25]. The flesh was then cut into small squares using a testing tool, and mechanical measurements and parameter calibrations were conducted within 12 h of specimen collection, as shown in Figure 6. The key intrinsic parameters of the specimens were determined as follows: (1) shape and size—the majority of melon seeds exhibited an oval shape, with dimensions of length, width, and thickness measured, resulting in an average size of 18.05 × 11.75 × 3.56 mm; the dimensions of the melon flesh in all directions after crushing were approximated to be 10 mm, and it was set to be a square of 10 × 10 × 10 mm; (2) density—the volume and mass were measured using the toluene specific gravity bottle method to calculate the density values of both melon seeds and flesh; (3) Poisson's ratio and shear modulus—the TA.XT Express C-type mass tester instrument (comprising computer mainframe, monitor, knife, vernier calipers, electronic balance, hygrometer, and thermometer), shown in Figure 7, was employed to conduct tests on both melon seeds and flesh. The compression test was conducted using the P-35 compression probe of the mass tester instrument, as shown in Figure 8. The data from the compression force–time curve were analyzed using Texture Exponent software 2020 to calculate the modulus of elasticity of both the melon seeds and flesh. The puncture test was conducted using the P-2 probe of the mass tester instrument, as shown in Figure 9. The data from the shear force–displacement curve were examined using Texture Exponent

software to determine the shear modulus. Subsequently, Poisson's ratio was then calculated. Additionally, the standard material of the separation roller in the seed–flesh separation device was identified as 304 stainless steel, and its intrinsic parameters were extracted using data consultation. The above intrinsic parameters are listed in Table 2.

(**a**) (**b**)

Figure 6. Test samples. (**a**) Melon seeds samples. (**b**) Melon flesh sample.

Figure 7. TA.XT express C-type mass tester.

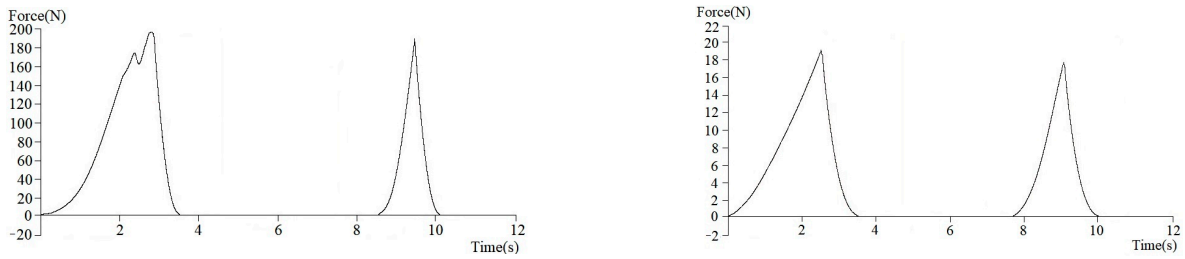

(**a**) (**b**)

Figure 8. Compression test force−time diagram of melon seeds and flesh. (**a**) Melon seeds. (**b**) Melon flesh.

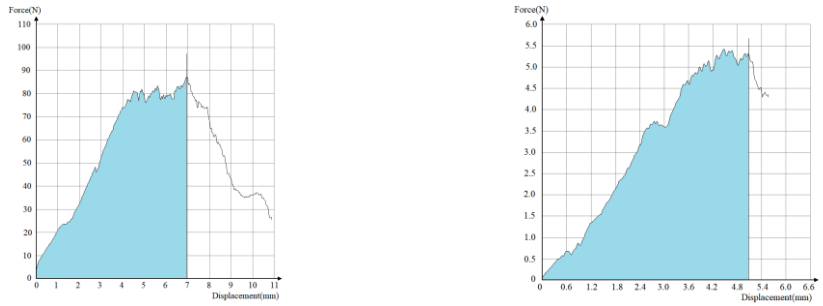

(**a**) (**b**)

Figure 9. Puncture test force−displacement diagram of melon seeds and flesh. (**a**) Melon seeds. (**b**) Melon flesh.

Table 2. Intrinsic parameters.

Materials	Parameters	Numerical Value
Melon seeds	Density (kg·m^{-3})	1028.4
	Poisson's ratio	0.35
	Elastic modulus (MPa)	4.66
	Shear modulus (MPa)	1.72
Melon flesh	Density (kg·m^{-3})	995.8
	Poisson's ratio	0.47
	Elastic modulus (MPa)	4.57
	Shear modulus (MPa)	1.55
304 stainless steel	Density (kg·m^{-3})	2500
	Poisson's ratio	0.3
	Elastic modulus (MPa)	194
	Shear modulus (MPa)	2.55

2.3.2. Calibration of Contact Parameters

The contact parameters between melon seeds, melon flesh, and separation roller device (304 stainless steel) were calibrated using discrete element simulation tests. Because of the interactions that occur between the seed melon components and the separation roller device. Therefore, the contact parameters to be calibrated include the static friction coefficient, rolling friction coefficient, and recovery coefficient between the materials and the separation roller.

1. Between the materials of melon seeds and flesh

The study selected the Hertz–Mindlin with JKR contact model to establish a discrete elemental model of melon seeds and flesh, considering the adhesion phenomenon between the seed–flesh mixture during the separation process [26,27], as illustrated in Figure 4.

Before calibrating the contact parameters, an angle of repose (AoR) measurement test was conducted [18,28]. In this study, the angle of repose test was carried out using the cylinder lifting method. The results showed that optimal angle of repose values of 22.19° for melon seeds, 28.08° for melon flesh, and 25.33° for the seed–flesh mixture, which met the test requirements, where the calibrated values of the contact parameters between the components of the seed melon in the test are shown in Table 3.

Table 3. Calibration values of contact parameters.

Contact Material	Collision Recovery Coefficient	Static Friction Coefficient	Rolling Friction Coefficient	JKR Surface Energy (J·m^2)
Melon seeds–melon seeds	0.200	0.249	0.250	0.200
Melon flesh–melon flesh	0.100	0.332	0.114	1.271
Melon seeds–melon flesh	0.228	0.368	0.269	2.213

2. Between seed melon components and separation rollers

The Hertz–Mindlin (no slip) contact model was selected due to the absence of adhesive forces between the seed melon components and the separation roller material. A homemade photoelectric inductive platform model for determining the friction coefficient was created for testing. The tilt plate, made of the same 304 stainless steel as the separation rollers, is depicted in Figure 10. The static friction test and material sliding tests were carried out. Each test group is repeated ten times, and the average results are obtained to derive the calibration values for the contact parameters between the seed melon components (melon seeds, melon flesh) and the material of the separation rollers, which was 304 stainless steel, as shown in Table 4.

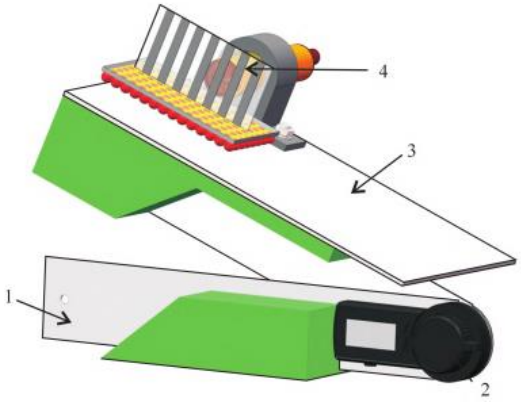

Figure 10. Homemade photoelectric sensing friction coefficient determination platform. (1) Bottom plate; (2) protractor; (3) tilt plate; and (4) photoelectric switch.

Table 4. Calibrated values of contact parameters between seed melon components and separation roller material.

Seed Melon Components–Separation Roller Material	Coefficient of Static Friction	Coefficient of Sliding Dynamic Friction	Coefficient of Collision Recovery
Melon seeds–304 stainless steel	0.207	0.753	0.361
Melon flesh–304 stainless steel	0.345	0.150	0.100

2.4. Simulation Design

2.4.1. Simulation Analysis and Effectiveness Validation in the Original Working State

The discrete element method (DEM 2022) software was employed to simulate the operational process of the seed–flesh separation device using the original parameters. The initial state of the simulation is illustrated in Figure 11a, while the progression of the simulation is depicted in Figures 11b–d and 12. The equation was calculated as shown in Equation (1) with the melon seed impurity rate as the response variable.

$$G_1 = \frac{M_1}{M_{t1}} \times 100\% \quad (1)$$

where G_1 is the melon seed impurity rate (%); M_1 is the mass of impurities in melon seeds (kg); and M_{t1} is the total mass of melon seeds containing impurities (kg).

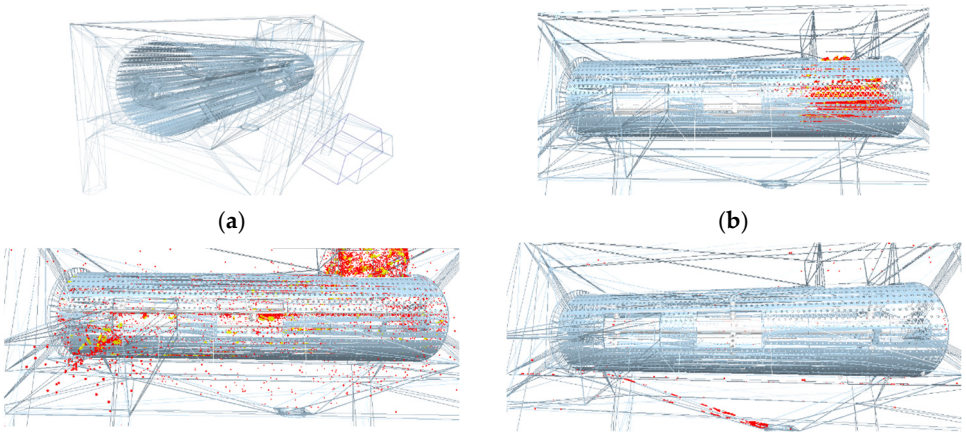

Figure 11. Simulation process of seed–flesh separation. (**a**) The initial state of simulation modeling; (**b**) t = 0.2 s; (**c**) t = 0.5 s; and (**d**) t = 1.0 s.

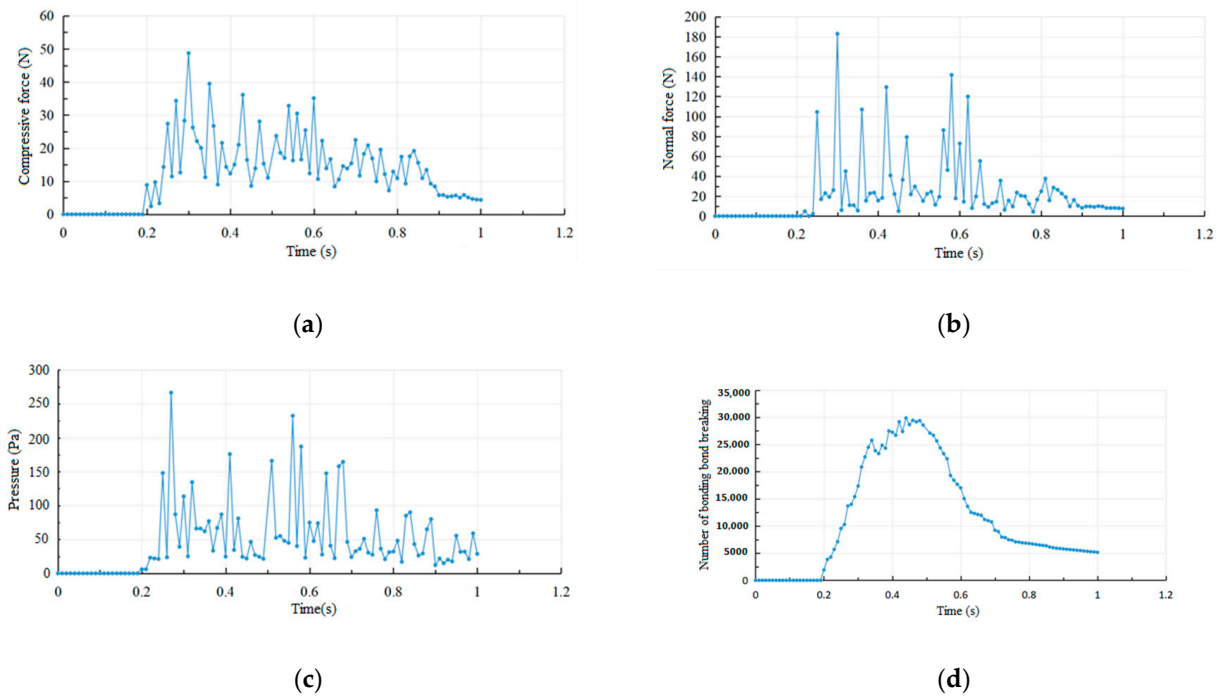

Figure 12. Time plot of each metric during simulation time. (**a**) Compression force−time curve of seed–flesh mixture; (**b**) parallel bond normal force−time curve; (**c**) separation roller scraper pressure–time curve; and (**d**) number of bonding bond breaking–time curve.

Because the seed–flesh separation process in this paper is the follow-up work of skin–flesh separation process in the seed-melon crushing and seed-extraction separator, according to the research results of the group's previous work, and considering the efficiency of the seed–flesh separator device, the final selection of seed–flesh mixture feeding volume of 10 kg, comprising 2 kg of seed particles and 8 kg of flesh particles were established in the particle factory, and the DEM simulation model established was shown in Figures 4 and 5. Tables 1 and 5 present the initial structural and kinematic parameters of the melon seeds-flesh separation device, while Tables 2–4 outline the intrinsic parameters and contact parameters. A discrete element simulation test was conducted on the seed–flesh separation device, followed by a production test on the prototype under the same parameters. Both the simulation and prototype tests were repeated three times, and the average values were used to calculate the impurity rate of melon seeds. The results, displayed on the right side of Table 5, compared the values of the simulation with those of the prototype to validate the accuracy of the simulation.

Table 5. Comparison of the results of real tests and simulation tests.

Factors	Separation Roller Speed ($r \cdot min^{-1}$)	Spacing between Scraper and Screen (mm)	Separation Roller Scraper Inclination Angle (°)	Melon Seed Impurity Rate (%)		
				Test Values	Simulation Values	Relative Errors
Numerical value	110	3	5	3.77	3.90	3.33

2.4.2. Design of Simulation Experiment

The primary components of the seed–flesh separation device consist of the separating roller and the screen. During simulation, the separating roller is modeled as a dynamic element, rotating around the central axis, while the remaining components, such as the screen, remain static. The simulation was conducted with a step size of 1.00×10^{-6} s, and a total time of 1 s was designated to model the motion and segregation of the seed–flesh

mixture in the seed–flesh separation apparatus. Through the high-speed operation of the separation roller, the seed–flesh mixture was separated under the axial and circumferential forces of the scraper. Therefore, the rotational speed of the separation roller, the spacing between the scraper and the screen, and the inclination angle of the scraper of the separation roller were selected as the influencing factors in this study, and the experimental values were taken, as shown in Table 6. The optimal structural parameters of the seed–flesh separating device were determined through one-factor testing and three-factor three-level orthogonal testing methods, with the melon seed impurity rate and the melon seed scratch rate as the evaluation criteria. The melon seed scratch rate is calculated by Equation (2):

$$G_2 = \frac{M_2}{M_{t2}} \times 100\% \quad (2)$$

where G_2 is the melon seed scratch rate (%); M_2 is the mass of scratched melon seeds in the sample (kg); and M_{t2} is the total mass of melon seeds in the sample (kg).

Table 6. Experimental factors.

Experimental Factors	Retrieve Value		
Separation roller speed (r·min^{-1})	70	110	150
Spacing between scraper and screen (mm)	1	3	5
Separation roller scraper inclination angle (°)	0	5	10

2.5. Field Test Method

The test of the seed melon crushing and seed-extraction separator independently developed by our team was conducted at the laboratory of the School of Electrical and Mechanical Engineering, Gansu Agricultural University, in Lanzhou City, Gansu Province. The experiment took place at a controlled temperature of 22 ± 1 °C and a humidity level of 20 ± 1%, as depicted in Figure 13.

Figure 13. Seed melon crushing and seed-extraction separator and test process.

During the experiment, the seed melon was manually loaded into the feeding hopper, with precise control over the feeding quantity. The separation roller speed, the spacing between the scraper and the screen, and the separation roller scraper inclination angle were adjusted in accordance with the predetermined test factors (Table 6), and no other conditions were changed during the experiment. At the end of the test, the collection box containing melon seeds and flesh, respectively, were moved from the discharge port of the seed–flesh separation device to the laboratory operating platform, and the melon seed impurity rate and the melon seed scratch rate were counted.

3. Simulation Results Analysis

3.1. Discrete Element Simulation Analysis of Seed–Flesh Separation Process

The seed–flesh separation process in the seed–flesh separation device was simulated, as illustrated in Figure 11. In order to enhance the visualization of the seed–flesh separation effect, the melon seed particles were represented in yellow, the melon flesh in red, and the separation device in the default color. A grid box group was established in the melon seed discharge port in the discrete element method (DEM) post-processing interface. Subsequently, the impurity rate and scratch rate of melon seeds were obtained through statistical calculations upon completion of the simulation, as depicted in Figure 11a. The simulation progress of the separation is illustrated in Figure 11b–d.

At t = 0.2 s, the seed–flesh mixture entered the screen through the inlet and underwent compression by the separating roller without separation occurring, as depicted in Figure 11b. By t = 0.5 s, as the separating roller rotated, the seed–flesh mixture underwent separation from the melon seeds and flesh along the axial and circumferential directions of the screen due to the collision with the scraper. Some melon flesh was discharged through the mesh of the screen into the melon juice outlet, while the melon seeds exited through the melon seed outlet, as illustrated in Figure 11c. By t = 1.0 s, the process of seed–flesh separation was mostly complete, with only a small quantity of melon seeds and flesh particles remaining in the screen and outlet, as shown in Figure 11d. Throughout the simulation, the majority of melon flesh broke down smoothly and flowed into the melon juice outlet through the sieve mesh, with only a minor portion of melon flesh particles crossing over into the melon seed outlet along with the seeds.

Figure 12a–c shows the time change curve of the compression force for the seed–flesh mixture model, the normal force for the parallel bond, and the force of the separating roller scraper during the operation of the separation device. By analyzing these curves collectively, it is evident that the peak values occur within the time range of 0.2 s to 0.7 s, suggesting that the simulation aligns with practical operational requirements. Through the utilization of Equation (1), the simulation enables the calculation of the melon seed impurity rate. Subsequently, based on the simulation parameters, statistical data presented in Table 5 indicate a relatively low relative error of 3.33% between the simulated and experimental values. This discrepancy signifies the effectiveness of the simulation testing process.

The separation efficiency of the seed–flesh mixture model is depicted by the number of broken bonds between particles, as illustrated in Figure 12d. Initially, when the seed–flesh mixture model is not in contact with the separation roller scraper, the number of separations is zero. As the operation progresses, the particles experience the impact force of the separation roller scraper and the squeezing force, causing an incremental breakage of bonding bonds, this trend exhibits a positive correlation. After a certain point of separation, the number of bonding bonds no longer changes. This is due to the centrifugal force exerted on the particles, leading to some of them being trapped in the gap between the scraper and the screen mesh without being separated. The bonding bonds between the particles remain in a stable state. The graph depicting the evolution of bonding bonds between particles mirrors the separation process of the model, aligning closely with the simulation process.

3.2. Analysis of the Influence of Factors on the Effect of Seed–Flesh Separation

3.2.1. The Influence of Separation Roller Speed on the Efficiency of Seed–Flesh Separation

In this study, the simulation experiment was conducted with varying separation roller speeds of 70 r/min, 110 r/min, and 150 r/min, while other conditions were maintained at the initial motion parameters specified in Table 5. Figure 14a,b illustrates the changes in melon seed impurity rate and scratch rate as the speed of the separating roller increases. The simulation results show that, as shown in Figure 14a, overall, as the separation roller speed increases, the melon seed impurity rate initially decreases rapidly, followed by a slow and gentle trend of change. Specifically, the melon seed impurity rate decreased rapidly as the speed increased from 70 r/min to 110 r/min, and then the rate of decrease slowed as it further increased to 150 r/min, eventually stabilizing. As shown in Figure 14b, the

melon seed impurity rate exhibited a consistent increase, rising slowly between 70 r/min and 110 r/min and more rapidly between 110 r/min and 150 r/min.

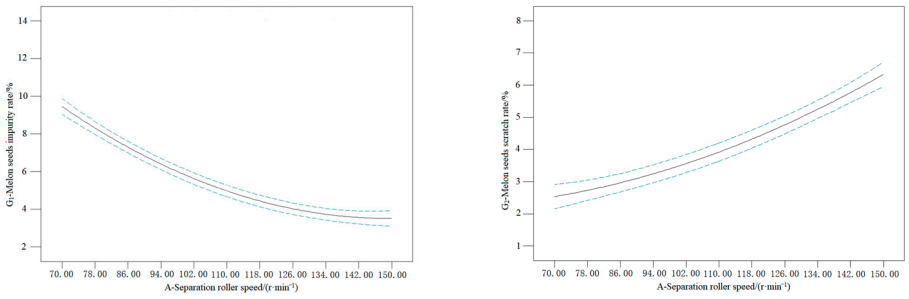

(**a**) (**b**)

Figure 14. Simulation test results of separation roller speed. (**a**) Trend of melon seed impurity rate. (**b**) Trend of melon seed scratch rate.

3.2.2. The Influence of the Spacing between Scraper and Screen on the Effectiveness of Seed–Flesh Separation

The simulation experiment was conducted in five scenarios with varying spacing between the scraper and the screen of 1 mm, 3 mm, and 5 mm, while keeping other conditions consistent with the initial motion parameters presented in Table 5. Figure 15a,b illustrate the trends in melon seed impurity rate and melon seed scratch rate as the spacing between the scraper and the screen increases. The simulation findings reveal, as shown in Figure 15a, that as the spacing between the scraper and the sieve mesh widens, the melon seed impurity rate shows an overall increasing trend. The rate of increase is relatively gradual, particularly between 1 mm and 3 mm, and slightly accelerates between 3–5 mm. As shown in Figure 15b, the melon seed scratch rate demonstrates an overall declining pattern, with a slower decrease observed within the 1–3 mm gap range and a more pronounced decrease within the 3–5 mm range.

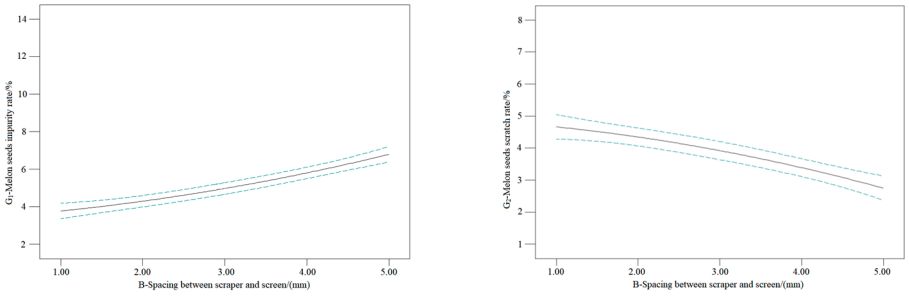

(**a**) (**b**)

Figure 15. Simulation test results of the spacing between scraper and screen. (**a**) Trend of melon seed impurity rate. (**b**) Trend of melon seed scratch rate.

3.2.3. The Influence of Separation Roller Scraper Inclination Angle on the Effectiveness of Seed–Flesh Separation

The simulation experiment was conducted in three different scenarios with separation roller scraper inclination angles of 0°, 5° and 10°. The initial motion parameters are detailed in Table 5. Figure 16a,b illustrates the trends in melon seed impurity rate and melon seed scratch rate as the separation roller scraper inclination angle increases. The analysis of the simulation results reveals, as shown in Figure 16a, that there is a subtle decrease in the melon seed impurity rate overall as the scraper's inclination angle increases. As shown in Figure 16b, the melon seed scratch rate exhibits a slight increase with the inclination angle, eventually leveling off.

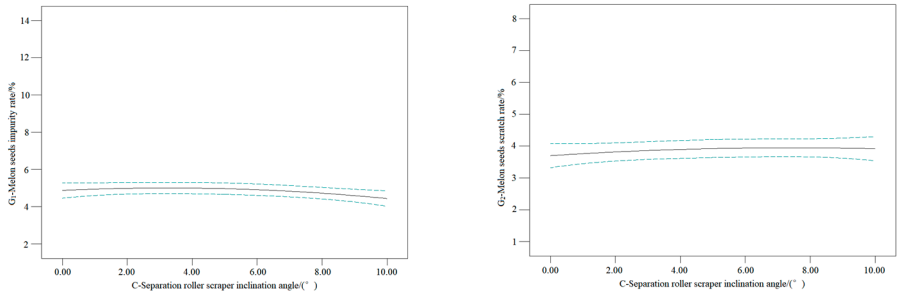

(**a**) (**b**)

Figure 16. Simulation test results of the separation roller scraper inclination angle. (**a**) Trend of melon seed impurity rate. (**b**) Trend of melon seed scratch rate.

3.3. Response Surface Test

3.3.1. ANOVA of Influencing Factors

A three-way analysis of variance (ANOVA) with a significance level of 0.05 was conducted to assess the impacts of separation roller speed, spacing between the scraper and screen, and scraper inclination on the melon seed impurity rate and the melon seed scratch rate. The factor coding for the response surface test is presented in Table 7, while the design and results of the response surface test are detailed in Table 8. The results of the ANOVA for melon seed impurity rate can be found in Table 9, and the results of the ANOVA for the scratching rate of melon seeds are shown in Table 10.

Table 7. The factor coding for the response surface test.

Level	A-Separation Roller Speed ($r \cdot min^{-1}$)	B-Spacing Between Scraper and Screen (mm)	C-Separation Roller Scraper Inclination Angle (°)
1	70	1	0
0	110	3	5
−1	150	5	10

Table 8. The design and results of the response surface test.

Test Number	A-Separation Roller Speed	B-Spacing Between Scraper and Screen	C-Separation Roller Scraper Inclination Angle	G_1-Melon Seed Impurity Rate/%	G_2-Melon Seed Scratch Rate/%
1	−1	−1	0	7.55	3.57
2	1	−1	0	2.63	7.05
3	−1	1	0	12.20	1.28
4	1	1	0	4.80	4.98
5	−1	0	−1	9.37	2.20
6	1	0	−1	3.59	6.10
7	−1	0	1	8.68	2.44
8	1	0	1	3.05	6.55
9	0	−1	−1	3.74	4.21
10	0	1	−1	6.46	2.89
11	0	−1	1	3.58	4.63
12	0	1	1	6.10	2.65
13	0	0	0	4.68	3.79
14	0	0	0	5.11	4.16
15	0	0	0	5.03	3.56
16	0	0	0	5.05	4.09
17	0	0	0	4.99	4.01

Table 9. ANOVA of melon seed impurity rate.

Source	Sum of Squares	Degree of Freedom	F Value	*p* Value	Significant Degree
Regression model	100.97	9	132.51	<0.0001	**
A	70.39	1	831.38	<0.0001	**
B	18.18	1	214.73	<0.0001	**
C	0.38	1	4.52	0.0710	/
AB	1.54	1	18.16	0.0037	**
AC	5.625×10^{-3}	1	0.066	0.8040	/
BC	0.01	1	0.12	0.7412	/
A^2	9.64	1	113.81	<0.0001	**
B^2	0.41	1	4.79	0.0649	/
C^2	0.41	1	4.85	0.0635	/
Residual	0.59	7			
Lack of fit terms	0.48	3	5.59	0.0648	/
Error	0.11	4			
Total variation	101.56	16			

Note: "**" indicates that the value is highly significant; * indicates that the value is significant; / indicates that the value is not significant.

Table 10. ANOVA of melon seed scratch rate.

Source	Sum of Squares	Degree of Freedom	F Value	*p* Value	Significant Degree
Regression model	0.24	9	31.64	<0.0001	**
A	0.15	1	183.19	<0.0001	**
B	0.057	1	68.40	<0.0001	**
C	2.502×10^{-4}	1	0.30	0.6014	/
AB	0.020	1	23.96	0.0018	**
AC	9.860×10^{-5}	1	0.12	0.7414	/
BC	5.927×10^{-4}	1	0.71	0.4277	/
A^2	1.924×10^{-3}	1	2.30	0.1732	/
B^2	4.457×10^{-3}	1	5.33	0.0543	*
C^2	1.352×10^{-6}	1	1.616×10^{-3}	0.9691	/
Residual	5.855×10^{-3}	7			/
Lack of fit terms	4.798×10^{-3}	3	6.05	0.0573	/
Error	1.057×10^{-3}	4			/
Total variation	0.24	16			/

Note: "**" indicates that the value is highly significant; * indicates that the value is significant; / indicates that the value is not significant.

According to the results in Tables 9 and 10, the *p*-values of the melon seed impurity rate regression model and melon seed scratch rate regression model are both smaller than 0.0001, less than the classical confidence level of 0.05, indicating that the linear relationship assumed by the models meets the requirements and that there is a significant difference with statistical significance [5,29,30].

After conducting a linear regression analysis of the model, the adequacy of the regression model coefficients was assessed, and the value range is [0,1]. The closer the coefficient is to 1, the better the fit of the model. The results show that the determination coefficient of the model of the melon seed impurity rate R^2 is 0.9942, while the determination coefficient of the model of the melon seed scratch rate R^2 is 0.9760, indicating the accuracy of the regression models.

Underfitting is an indication of a poor model. If the *p*-value of the lack of fit is greater than 0.05, it indicates that the lack of fit is not significant. The *p*-value of the lack of fit for the regression model of melon seed impurity rate is 0.0648 in Table 9, and the *p*-value of the

misfit term for the regression model of melon seed scratch rate in Table 10 is 0.0573, both of which are greater than 0.05, and the lack of fit term is insignificant, which indicates that there are no other factors in the model that have an impact on the values of melon seed impurity rate and melon seed scratch rate. The standard residual error of the regression is analyzed using Design Expert software 10, which satisfies the hypothesis of normality and normal distribution, and the variance is equal, indicating that the model is stable and valid, as shown in Figure 17a,b.

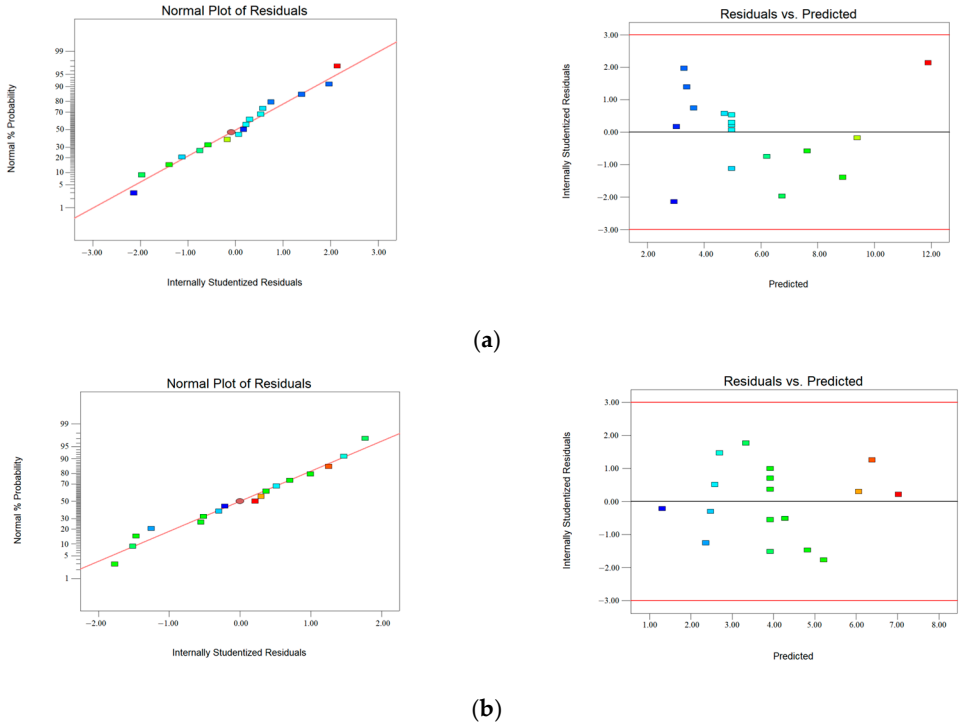

Figure 17. Standard residual error of the regression models. (**a**) Standard residual verification of the melon seed impurity rate; and (**b**) Standard residual verification of the melon seed scratch rate.

For further analysis, it can be seen from Table 9 that the effects of single factor A (separation roller speed), B (spacing between scraper and screen), interaction item AB, and secondary item A^2 on the melon seed impurity rate were extremely significant, and the effects of single factor C (separation roller scraper inclination angle), interaction item AC and BC, and secondary item B^2 and C^2 are less significant. It can be seen from Table 10 that the effects of single factor A (separation roller speed), B (spacing between scraper and screen), and interaction item AB on the melon seed scratch rate were extremely significant, and secondary item B^2 has a more significant effect on melon seed scratch rate, and the other items have a smaller effect.

Under the premise of ensuring that the fitted regression model was optimally fitted, the experimental data underwent multiple regression analysis to obtain optimal regression equations for G_1 (melon seed impurity rate) and G_2 (melon seed scratch rate) after eliminating non-significant factors, as presented in Equations (3) and (4).

$$G_1 = 4.97 - 2.97A + 1.51B - 0.62AB + 1.51A^2 \quad (3)$$

$$G_2 = 0.5 - 0.14A - 0.085B + 0.071AB + 0.033B^2 \quad (4)$$

3.3.2. Separation Performance Analysis

The response surfaces of the interaction factors to the test indexes of the melon seed impurity rate and melon seed scratch rate are shown in Figure 18.

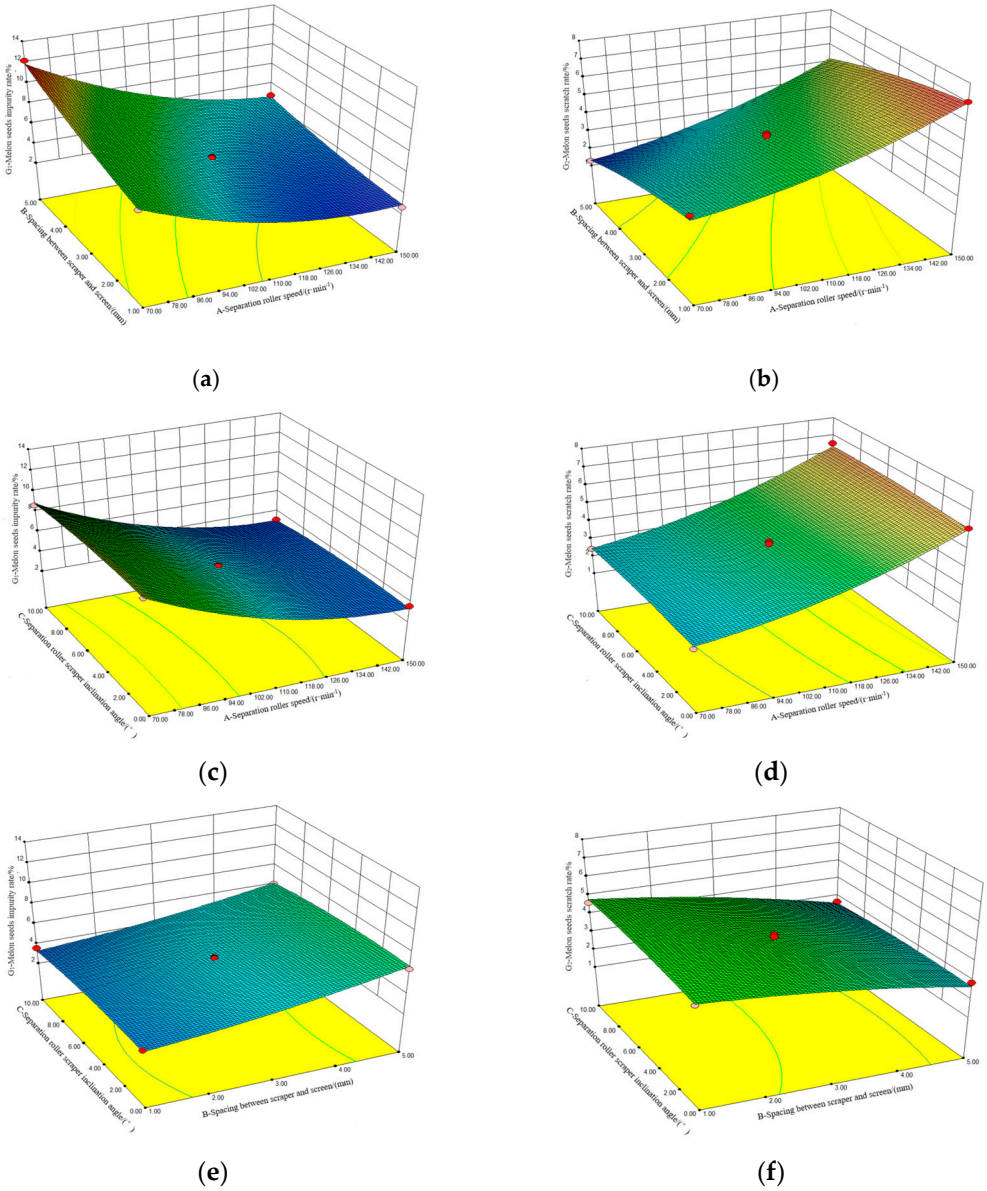

Figure 18. Influence of the interaction effect of the separation device working parameters on melon seed impurity rate and melon seed scratch rate. (**a**) Influence of separation roller speed and spacing between scraper and screen on melon seed impurity rate; (**b**) influence of separation roller speed and spacing between scraper and screen on melon seed scratch rate; (**c**) influence of separation roller speed and separation roller scraper inclination angle on melon seed impurity rate; (**d**) influence of separation roller speed and separation roller scraper inclination angle on melon seed scratch rate; (**e**) influence of spacing between scraper and screen and separation roller scraper inclination angle on melon seed impurity rate; and (**f**) influence of spacing between scraper and screen and separation roller scraper inclination angle on melon seed scratch rate.

As shown in Figure 18a,b, as the rotational separation roller speed increases and the spacing between the scraper and screen decreases, the melon seed impurity rate decreases, and the melon seed scratch rate increases. This was because the elevation in the separation roller speed amplifies the force exerted by the separation roller scraper on the seed–flesh mixture, leading to a shorter duration for seed–flesh separation, thus enhancing work efficiency. Simultaneously, the reduced spacing between the scraper and screen augments the contact area between the scraper and the seed–flesh mixture, increasing the number of crushing effects on the seed–flesh mixture, intensifying the squeezing effect, and ensuring

a more thorough separation, consequently decreasing the impurity rate in melon seeds. However, the increased force on the melon seeds in the mixture exposes them to greater impact, extrusion, and friction forces, while the decreased spacing results in more frequent impacts and extrusions on the seeds. Ultimately and simultaneously, this led to an increase in the number of scratched melon seeds and an increase in the rate of melon seed scratching.

As shown in Figure 18c,d, the separation roller scraper inclination angle has a significant impact on the axial conveying capacity of the separation roller. When the inclination angle is too small, the axial conveying capacity is poor, resulting in the seed–flesh mixture being predominantly separated at the front part of the screen mesh. This scenario hinders the effective utilization of the middle and back sections of the screen mesh, leading to easy clogging, reduced separation efficiency, and poor working efficiency. Conversely, the inclination angle that is too large causes the seed–flesh mixture in the front section of the screen mesh to be ejected in the circumferential direction, while moving rapidly backward along the axial direction, making the most of the mixture to be separated in the middle and back sections of the screen mesh. At the same time, there will be a large number of mixtures without the full effect of the separation rollers reaching the melon seeds screen outlet. The considerable amount of the mixture not being fully separated will flow out from the melon seeds screen mesh outlet, and the separation was not complete, thus increasing the melon seed impurity rate. Therefore, while choosing the appropriate scraper inclination angle, appropriately increase the separation roller speed. This approach enables the seed–flesh mixture in the sieve screen to undergo a spiral movement driven by centrifugal and axial forces, resulting in enhanced separation efficiency and a notable reduction in melon seed impurity rate. Nonetheless, the intensified movement and increased force may elevate the risk of melon seed scratches to a certain extent, resulting in an increased melon seed scratch rate. The response surface analysis indicates that the separation roller scraper inclination angle relative to the separation roller speed has a minor impact on the impurity rate and scratch rate of the melon seeds.

As shown in Figure 18e,f, the interaction between the scraper–screen mesh spacing and separation roller scraper inclination angle did not heavily impact the impurity rate or scratch rate of melon seeds. However, comparatively, the influence of scraper–screen mesh spacing was more pronounced than that of separation roller scraper inclination angle. Within the range of values, an increase in the spacing between the scraper and screen, as well as in the separator roller scraper inclination angle, resulted in a gradual rise in the melon seed impurity rate and a gradual decline in the melon seed scratch rate.

3.4. Optimal Parameter Design

The optimal parameter combination was determined by the action rules of each working parameter on the melon seed impurity rate and melon seed scratch rate. The parameter optimization design was carried out by Design Expert, and the optimization rules are shown in Equations (5) and (6) as follows.

$$\text{Optimization objective: } \min(G_1, G_2)$$

$$\left\{ \begin{array}{c} 2.63 \le G_1 \le 12.20 \\ 1.28 \le G_2 \le 7.05 \end{array} \right\} \tag{5}$$

$$\text{Design variables were A, B, C}$$

$$\text{s.t} \begin{cases} 70 \le \text{A} \le 150 \\ 1 \le \text{B} \le 5 \\ 0 \le \text{C} \le 10 \end{cases} \tag{6}$$

The optimal working parameters of the seed–flesh separation process obtained after optimization are as follows: the separating roller speed was 117.53 r/min, the spacing between the scraper and the screen was 5 mm, and the separation roller scraper inclination

angle was 10°. The corresponding test evaluation indexes obtained were as follows: the melon seed impurity rate was 5.59%, and the melon seed scratch rate was 2.85%.

3.5. Prototype Separating Operation Test Verification

To validate the optimization outcomes, the optimal working parameters were utilized as the operational settings for the seed–flesh separation device prototype of the seed-melon crushing and seed-extraction separator. A series of ten separation effect tests were conducted in the laboratory, with the melon seed impurity rate and the melon seed scratch rate serving as evaluation criteria. These tests aimed to confirm the validity of the simulation results. The schematic of the seed–flesh separation device test prototype is illustrated in Figure 13. During operation, a 10 kg seed–flesh mixture is fed through the inlet into the working drum for separation. Upon completion of each test, the melon seed impurity rate and melon seed scratch rate were recorded at the outlet, as displayed in Figure 19. Each test iteration is performed thrice, and the average values are calculated.

(**a**) (**b**) (**c**)

Figure 19. Prototype separating operation test results. (**a**) Statistics on the melon seed impurity rate; (**b**) statistics on the melon seed scratch rate; and (**c**) melon flesh after separation.

The results show that the average impurity rate and scratch rate of melon seeds in the prototype test are 5.71% and 2.91%, respectively. The relative errors compared to the simulation values are 2.15% and 2.11%, respectively, attributed to uncontrollable and unknown environmental factors. When viewing them comprehensively, there is minimal disparity between the simulation and prototype test data. The optimized working parameters notably enhance the efficiency of seed–flesh separation, achieving a harmonious balance between reducing the impurity rate and scratch rate of melon seeds. Consequently, the seed–flesh separation device of the melon crushing and seed-extraction separator, as designed in this study, demonstrates significantly improved performance after parameter optimization. These results are further validated and analytically substantiated through field tests, yielding more precise and elucidating outcomes.

4. Conclusions

This study took the seed–flesh separating device of the seed -melon crushing and seed-extraction separator developed by the group as the research object and established a discrete element model of melon seeds, melon flesh, and the seed–flesh separating device. Five contact parameters between melon seeds, melon flesh, and the separating device were calibrated. Then, the seed–flesh separating process was simulated and analyzed using the discrete element method (DEM). Design Expert software 10 was used to carry out a one-factor simulation and a three-factor three-level orthogonal test on the factors influencing the efficiency of seed–flesh separation to obtain the optimized working parameter values and corresponding evaluation index optimal values. Finally, the simulation results were validated through prototype testing of the seed–flesh separation device of the seed melon crushing and seed-extraction separator. The study reveals the following specific conclusions:

(1) Aiming at the industrial bottleneck of poor seed–flesh separation and high rate of impurity and scratches in melon seeds in traditional seed melons, the group proposes a seed melon crushing and seed-extraction separator that realizes seed–flesh separation automatically and efficiently. Meanwhile, the discrete element model of melon seeds, melon flesh, and seed–flesh separating device was established by using DEM, and the contact parameters between melon seeds–melon seeds, melon flesh–melon flesh, and melon seeds–melon flesh materials were calibrated with the experimental angle repose as the optimization target value, as well as the contact parameters between melon seeds, melon flesh, and the material of separating rollers (304 stainless steel) were calibrated by using the homemade photoinductive friction coefficient determination platform.

(2) The discrete element method (DEM) was used to analyze the one-factor simulation of separation roller speed (A), spacing between scraper and screen (B), and separation roller scraper inclination angle (C), and the investigated impact of the three factors on the efficiency of seed–flesh separation was explored by taking melon seed impurity rate (G_1) and melon seed scratch rate (G_2) as evaluation indexes.

(3) The three-factor, three-level orthogonal test conducted on the seed–flesh separation process revealed that with separation roller speed (A) set at 117.53 r/min, spacing between scraper and screen (B) set at 5 mm, and separation roller scraper inclination angle (C) set at 10°, melon seed impurity rate (G_1) was 5.59%, and melon seed scratch rate (G_2) was 2.85%. Subsequent laboratory prototype testing indicated that under the optimized parameters, the average values for melon seed impurity rate (G_1) and melon seed scratch rate (G_2) were 5.71% and 2.91%, respectively. The relative errors compared to the simulated values were found to be 2.15% and 2.11%, respectively. These results indicate a comprehensive enhancement in the seed–flesh separation process, achieved through a balanced approach focusing on minimizing both melon seed impurity rate and melon seed scratch rate.

Author Contributions: Conceptualization, F.W., L.P. and Q.L.; methodology, F.W., J.W. and X.H.; software, Q.L., Y.X. and X.M.; validation, L.P., S.L., G.M. and J.W.; formal analysis, S.L. and J.W.; investigation, S.L. and X.H.; writing—original draft preparation, Q.L.; writing—review and editing, F.W. and Q.L.; visualization, Q.L.; supervision, L.P.; project administration, G.M. and X.H. All authors have read and agreed to the published version of the manuscript.

Funding: This research was funded by the National Natural Science Foundation of China (51765003), the Educational Science and Technology Innovation Program of Gansu Province, China (2021CYZC-51), and Special Talent of Gansu Agricultural University (Grant No. GAU-KYQD-2020-15).

Data Availability Statement: The data presented in this study are available on request from the authors.

Acknowledgments: The authors thank the editor for providing helpful suggestions to improve the quality of this manuscript.

Conflicts of Interest: The authors declare no conflicts of interest.

References

1. Wang, H.W. The direction of research and production of seed melon in China through literature analysis. *Gansu Agric. Sci. Technol.* **2019**, *6*, 62–72.
2. Huang, X.P.; Xiong, S.L.; Wang, Q.H.; Sun, C.G.; Wan, F.X. Analysis of electrical characteristics of seed melon pericarp in different parts. *J. Anhui Agric. Univ.* **2022**, *49*, 514–520.
3. Ding, H.B.; Wu, L.; Zang, Z.P.; Xu, Y.R.; Huang, X.P.; Wu, J.F. Study on microwave vacuum drying characteristics and quality of seed melon solids. *J. Chin. Agric. Mech.* **2023**, *44*, 88–94.
4. Zhou, Y.H.; Lu, W.D.; Ma, X.L.; Gao, J.L.; Fan, X.Q.; Guo, J.F.; Chen, Y.Q.; Lin, M.; Shi, S.B. Phenotypic characters identification and gengtic diversity analysis of seed melon germplasm resources. *J. China Agric. Univ.* **2023**, *28*, 119–132.
5. Wu, J.; Tang, Q.; Mu, S.L.; Jiang, L.; Hu, Z.C. Test and optimization of oilseed rape (*Brassica napus* L.) threshing device based on DEM. *Agriculture* **2022**, *12*, 1580. [CrossRef]
6. Zhang, D.M.; Yi, S.J.; Zhang, J.H.; Bao, Y.H. Establishment of millet threshing and separating model and optimization of harvester parameters. *Alex. Eng. J.* **2022**, *61*, 11251–11265. [CrossRef]

7. Wang, Q.; Mao, H.; Li, Q. Modelling and simulation of the grain threshing process based on the discrete element method. *Comput. Electron. Agric.* **2020**, *178*, 105790. [CrossRef]
8. Coetzee, C.J.; Lombard, S.G. The destemming of grapes: Experiments and discrete element modelling. *Biosyst. Eng.* **2013**, *114*, 232–248. [CrossRef]
9. Li, X.P.; Zhang, W.T.; Wang, W.Z.; Huang, Y. Design and test of longitudinal axial flow staggered millet flexible threshing device. *Agriculture* **2022**, *12*, 1179. [CrossRef]
10. Ma, Z.; Li, Y.; Xu, L. Discrete-element method simulation of agricultural particles' motion in variable-amplitude screen box. *Comput. Electron. Agric.* **2015**, *118*, 92–99. [CrossRef]
11. Yu, C.; Lin, D.D.; Xu, N.N.; Wang, X.W.; Pu, K.W.; Wang, Z.H.; Zhao, G.F.; Geng, R.H.; Gong, S.P. DEM simulation of particle flow and separation in a vibrating flip-flow screen. *Particuology* **2023**, *73*, 113–127. [CrossRef]
12. You, Y.; Liu, M.L.; Ma, H.Q.; Xu, L.; Liu, B.; Shao, Y.L.; Tang, Y.P.; Zhao, Y.Z. Investigation of the vibration sorting of non-spherical particles based on DEM simulation. *Powder Technol.* **2018**, *325*, 316–332. [CrossRef]
13. Ghodki, M.B.; Kumar, K.C.; Goswami, T.K. Modeling breakage and motion of black pepper seeds in cryogenic mill. *Adv. Powder Technol.* **2018**, *19*, 1055–1071. [CrossRef]
14. Wang, Y.; Zhang, Y.T.; Yang, Y.; Zhao, H.M.; Yang, C.H.; He, Y.; Wang, K.; Liu, D.; Xu, H.B. Discrete element modelling of citrus fruit stalks and its verification. *Biosyst. Eng.* **2020**, *200*, 400–414. [CrossRef]
15. Su, Z.; Li, Y.M.; Dong, Y.H.; Tang, Z.; Liang, Z.W. Simulation of rice threshing performance with concentric and non-concentric threshing gaps. *Biosyst. Eng.* **2020**, *197*, 270–284. [CrossRef]
16. Horabik, J.; Molenda, M. Parameters and contact models for DEM simulations of agricultural granular materials: A review. *Biosyst. Eng.* **2016**, *147*, 206–225. [CrossRef]
17. Liu, F.Y.; Zhang, J.; Li, B.; Chen, J. Calibration of parameters of wheat required in discrete element method simulation based on repose angle of particle heap. *Trans. Chin. Soc. Agric. Eng.* **2016**, *32*, 247–253.
18. Song, X.F.; Dai, F.; Zhang, F.W.; Wang, D.M.; Liu, Y.C. Calibration of DEM models for fertilizer particles based on numerical simulations and granular experiments. *Comput. Electron. Agric.* **2023**, *204*, 107507. [CrossRef]
19. Rackl, M.; Hanley, K.J. A methodical calibration procedure for discrete element models. *Powder Technol.* **2017**, *307*, 73–83. [CrossRef]
20. Chen, Z.P.L.; Wassgren, C.; Veikle, E.; Ambrose, K. Determination of material and interaction properties of maize and wheat grains for DEM simulation. *Biosyst. Eng.* **2020**, *195*, 208–226. [CrossRef]
21. Ma, X.D.; Guo, B.J.; Li, L.L. Simulation and experiment study on segregation mechanism of rice from straws under horizontal vibration. *Biosyst. Eng.* **2019**, *186*, 1–13. [CrossRef]
22. Guan, Z.H.; Mu, S.L.; Jiang, T.; Li, H.T.; Zhang, M.; Wu, C.Y.; Jin, M. Development of centrifugal disc spreader on tracked combine harvester for oilseed rape under sowing rice based on DEM. *Agriculture* **2022**, *12*, 562. [CrossRef]
23. Makange, N.R.; Ji, C.; Torotwa, I. Prediction of cutting forces and soil behavior with discrete element simulation. *Comput. Electron. Agric.* **2020**, *179*, 105848. [CrossRef]
24. Lei, X.; Hu, H.; Wu, W.; Liu, H.; Liu, L.; Yang, W.; Zhou, Z.; Ren, W. Seed Motion Characteristics and Seeding Performance of a Centralized Seed Metering System for Rapeseed Investigated by DEM Simulation and Bench Testing. *Biosyst. Eng.* **2021**, *203*, 22–33. [CrossRef]
25. Sun, H.B.; Li, S.Y.; Huang, X.P.; Wu, J.F.; Wan, F.X. Discrete element model construction and seed-flesh separation process of seed gourd. *J. Northwest Agric. For. Univ. (Nat. Sci. Ed.)* **2022**, *50*, 144–154.
26. Schramm, M.; Tekeste, M.Z. Wheat straw direct shear simulation using discrete element method of fibrous bonded model. *Biosyst. Eng.* **2022**, *213*, 1–12. [CrossRef]
27. Guo, Y.; Chen, Q.S.; Xia, Y.D.; Westover, T.; Eksioglu, S.; Roni, M. Discrete element modeling of switchgrass particles under compression and rotational shear. *Biomass Bioenergy* **2020**, *141*, 105649. [CrossRef]
28. Li, P.; Ucgul, M.; Lee, S.H.; Saunders, C. A new approach for the automatic measurement of the angle of repose of granular materials with maximal least square using digital image processing. *Comput. Electron. Agric.* **2020**, *172*, 105356. [CrossRef]
29. Zhang, N.; Fu, J.; Chen, Z.; Chen, X.G.; Ren, L.Q. Optimization of the process parameters of an air-screen cleaning system for frozen corn based on the response surface method. *Agriculture* **2021**, *11*, 794. [CrossRef]
30. Li, X.Y.; Du, Y.F.; Guo, J.L.; Mao, E.R. Design, simulation, and test of a new threshing cylinder for high moisture content corn. *Appl. Sci.* **2020**, *10*, 4925. [CrossRef]